Ground-state correlations within a nonperturbative approach

G. De Gregorio,[1,2] J. Herko,[3] F. Knapp,[3] N. Lo Iudice,[1,2] and P. Veselý[4]
[1]*Dipartimento di Fisica, Università di Napoli Federico II, Naples, Italy*
[2]*INFN Sezione di Napoli, Naples, Italy*
[3]*Faculty of Mathematics and Physics, Charles University, Prague, Czech Republic*
[4]*Nuclear Physics Institute, Czech Academy of Sciences, 250 68 Řež, Czech Republic*
(Received 18 October 2016; revised manuscript received 20 January 2017; published 7 February 2017)

The contribution of the two-phonon configurations to the ground state of ^{4}He and ^{16}O is evaluated nonperturbatively using a Hartree-Fock basis within an equation-of-motion phonon method using a nucleon-nucleon optimized chiral potential. Convergence properties of energies and root-mean-square radii versus the harmonic oscillator frequency and space dimensions are investigated. The comparison with the second-order perturbation theory calculations shows that the higher-order terms have an appreciable repulsive effect and yield too-small binding energies and nuclear radii. It is argued that four-phonon configurations, through their strong coupling to two phonons, may provide most of the attractive contribution necessary for filling the gap between theoretical and experimental quantities. Possible strategies for accomplishing such a challenging task are discussed.

DOI: 10.1103/PhysRevC.95.024306

I. INTRODUCTION

A major objective in theoretical nuclear physics is to formulate methods able to determine the properties of finite nuclei starting from fundamental interactions among nucleons without relying on approximations or free parameters. They are expected to probe nuclear interactions and to predict properties not sufficiently explored experimentally.

Several *ab initio* approaches, often complementing one another, are available (see Ref. [1] for a review). Most of them, like the no-core shell model (NCSM) [2–4], coupled-cluster (CC) theory [5–10], and the in-medium similarity renormalization group (IM-SRG) [11–15], are focused on bulk and low-energy spectroscopic properties.

In the past, these and other first-principles methods adopted meson-exchange nucleon-nucleon potentials tuned on scattering phase-shift analysis and deuteron properties. An exhaustive list can be found in Refs. [1,4]. In recent years, they have been using potentials derived from chiral effective theory. This theory introduces naturally the three-body ($3N$) force through a power counting in the ratio Q/Λ of the momentum transfer Q over a cut-off Λ, which establishes a hierarchy of NN, $3N$, and many-body forces. A detailed discussion with the appropriate references can be found in Refs. [1,16].

As pointed out in Ref. [1], the $3N$ forces are crucial in determining the saturation properties of nuclear matter [17,18], affect the binding energies, radii, and low-lying spectroscopic properties of light nuclei [2,19], and describe the structure and the correct evolution of neutron-rich oxygen isotopes up to the drip line [7,20–23].

However, the main contribution comes from the density-dependent NN components the $3N$ forces induce [1]. Moreover, an optimized NN chiral potential NNLO$_{\rm opt}$ was derived [24] that reproduces the experimental binding energies and the drip line in neutron-rich oxygen isotopes. In calcium isotopes, it overestimates the binding energy but reproduces energy differences and shell closures.

Owing to the complex structure of the equations to be solved and the dimensions of the configuration space, most of these first-principles calculations are involved and confined to light and, in a few cases, medium-light nuclei.

To avoid these complications, a many-body perturbation theory (MBPT), using a $NN+3N$ chiral potential, was proposed recently as a much simpler and flexible alternative [25]. A calculation of the perturbation series up to 30th order, achieved by a resummation technique exploiting the Padé approximants [26], shows that a good convergence is obtained for ^{16}O already at the third order as long as a Hartree-Fock (HF), rather than a harmonic oscillator (HO), basis is adopted. Thus, calculations up to third order could be extended to a long chain of nuclei up to ^{132}Sn, yielding binding energies in good agreement with experiments. Analogous convergence properties were obtained in other third-order perturbation theory calculations using $V_{\rm lowk}$ [27], unitary correlation operator method [28], and, very recently, the two-body part of the chiral N^{3}LO as well as the J-matrix inverse scattering potential [29].

The suggestion that the perturbation series is rapidly convergent is very appealing. It needs, however, to be confirmed by nonperturbative calculations. These can be performed within an alternative approach where the Hamiltonian matrix is expanded in terms of the number of particle-hole configurations (np-nh) ($n=0,1,2,\ldots$). This expansion underlies approaches like CC theory [1,5] and IM-SRG [13,15].

The random-phase approximation (RPA) provides also a correlated ground state [30–32] incorporating many p-h configurations [33]. Only in a few cases, however, was it adopted to estimate the correlation energy [33–35]. Analogous investigations can be carried out in second RPA (SRPA) [36–40] or other extensions. To our knowledge, however, no calculations based on these approaches have been performed.

An explicit and systematic expansion in terms of correlated np-nh states is accomplished in an equation-of-motion phonon method (EMPM) proposed a few years ago [41,42]. In its upgraded version [43], the method constructs a set of equations

of motion which are solved iteratively to yield an orthonormal basis of n-phonon states $|\alpha_n\rangle$ ($n = 0,1,2,\ldots,n,\ldots$) built of phonons obtained in Tamm-Dancoff approximation (TDA). The basis is then adopted to solve the eigenvalue problem in the full multiphonon space. The formalism does not rely on approximations. The correlated nature of the constituent phonons, however, may allow for simplifying assumptions. It might be possible, for instance, to use a restricted number of basis states because the high-energy p-h configurations are incorporated practically in all TDA phonons.

The EMPM was adopted mainly to investigate the detailed properties of the dipole response in heavy neutron-rich doubly magic nuclei using a Nilsson [44] and a HF basis [45,46]. More recently, it was formulated in a Hartree-Fock-Bogoliubov (HFB) quasiparticle scheme and employed to study the low-lying spectrum as well as the dipole response of the neutron-rich ^{20}O [47].

Here, we exploit the method to study the ground-state properties. We evaluate the net contribution of two-phonon configurations to assess quantitatively the importance of the higher-order 2p-2h terms, fully accounted for by the EMPM, with respect to second-order perturbation theory. Moreover, by comparing the results with experiments, it is possible to assess the importance of more complex configurations, chiefly 4p-4h.

The calculation is performed in a HF basis using the two-body optimized chiral potential NNLO$_{\rm opt}$. We first study the convergence properties of the HF ground-state energies and radii in ^{4}He, ^{16}O, and ^{40}Ca versus the frequency ω and the dimensions of the HO space used to generate the HF basis. We then present a systematic of HF energies and radii covering a large part of the periodic table.

A thorough EMPM investigation of the convergence properties is carried out for ^{4}He and ^{16}O. An analogous study in heavier nuclei would require unbearably lengthy calculations or, alternatively, drastic truncations of the multiphonon space. How these truncations may be made reliably will be discussed.

II. BRIEF OUTLINE OF THE METHOD

The Hamiltonian considered here is composed of an intrinsic kinetic term $T_{\rm int}$ and a nucleon-nucleon (NN) potential V_{NN}. It has therefore the structure

$$H = T_{\rm int} + V_{NN} = T + V_{NN} + T_2, \tag{1}$$

where

$$T = \left(1 - \frac{1}{A}\right)\frac{1}{2m}\sum_i p_i^2 \tag{2}$$

is a modified one-body kinetic term and

$$T_2 = -\frac{1}{2mA}\sum_{i\neq j}\vec{p}_i\cdot\vec{p}_j \tag{3}$$

is a two-body kinetic piece. Once the HF basis is generated, H assumes the form

$$H = H_0 + V. \tag{4}$$

In second quantization, the one-body term takes the form

$$H_0 = \sum_r [r]^{1/2}\epsilon_r (a_r^\dagger \times b_r)^0, \tag{5}$$

where ϵ_r are the HF energies and $a_r^\dagger = a^\dagger_{x_r j_r m_r}$ and $b_r = (-)^{j_r+m_r} a_{x_r j_r -m_r}$ are particle creation and annihilation operators, respectively. We have put $[r] = 2j_r + 1$ and use this notation throughout the paper. The symbol $\times$ denotes coupling of two tensor operators to angular momentum Ω.

The two-body part becomes

$$V = -\frac{1}{4}\sum_{rstq\Omega}[\Omega]^{1/2} V^\Omega_{rstq}[(a_r^\dagger \times a_s^\dagger)^\Omega \times (b_t \times b_q)^\Omega]^0, \tag{6}$$

where V^Ω_{rstq} is unnormalized and antisymmetrized.

It is useful to write the latter potential in the recoupled form

$$V = \frac{1}{4}\sum_{rsqt\sigma}[\sigma]^{1/2} F^\sigma_{rsqt}[(a_r^\dagger \times b_s)^\sigma \times (a_q^\dagger \times b_t)^\sigma]^0, \tag{7}$$

where

$$F^\sigma_{rsqt} = \sum_\Omega [\Omega](-)^{r+t-\sigma-\Omega} W(rsqt;\sigma\Omega) V^\Omega_{rqst} \tag{8}$$

and $W(rsqt;\sigma\Omega)$ are Racah coefficients.

A. p-h Tamm-Dancoff

The preliminary step is the solution of the TDA eigenvalue equations

$$\langle 0|\left[\overline{(a_{\rm p}^\dagger \times a_{\rm h})^\lambda_{\rm ph}}, H\right]^\lambda|\lambda\rangle = (E_\lambda - E_0)c^\lambda_{\rm ph}, \tag{9}$$

where

$$c^\lambda_{\rm ph} = \langle({\rm p}\times{\rm h})^\lambda|\lambda\rangle = \langle 0|\overline{(a_{\rm p}^\dagger \times a_{\rm h})^\lambda_{\rm ph}}|\lambda\rangle \tag{10}$$

and the overline symbol denotes the adjoint of a tensor operator.

After expanding the commutator, we obtain

$$\sum_{\rm p'h'} A^\lambda_{\rm php'h'} c^\lambda_{\rm p'h'} = (E_\lambda - E_0)c^\lambda_{\rm ph}, \tag{11}$$

where

$$A^\lambda_{\rm php'h'} = (\epsilon_{\rm p} - \epsilon_{\rm h})\delta_{\rm pp'}\delta_{\rm hh'} + F^\lambda_{\rm phh'p'}. \tag{12}$$

The solution of the eigenvalue equation yields the TDA eigenvalues and eigenvectors of the form

$$|\lambda\rangle = O^\dagger_\lambda|0\rangle, \tag{13}$$

where

$$O^\dagger_\lambda = \sum_{\rm ph} c^\lambda_{\rm ph}(a_{\rm p}^\dagger \times a_{\rm h})^\lambda \tag{14}$$

is the TDA phonon operator.

The TDA wave functions can be used to compute the density matrix

$$\rho_{\lambda\lambda'}([r\times s]^\sigma) = \langle\lambda'\|(a_r^\dagger \times b_s)^\sigma\|\lambda\rangle = [\lambda\lambda'\sigma]^{1/2}\sum_t c^\lambda_{ts}c^{\lambda'}_{tr} W(\lambda' t\sigma s; r\lambda). \tag{15}$$

Here t runs over particle ($t = \mathrm{p}$) or hole ($t = \mathrm{h}$) states, according that $(rs) = (\mathrm{hh}')$ or $(rs) = (pp')$, respectively.

For $J^\pi = 1^-$, we need to remove the spurious components induced by the center-of-mass (c.m.) motion. As discussed in Ref. [48], we eliminate these admixtures by Gramm-Schmidt orthogonalization of the p-h basis states to the c.m. state defined as

$$|\lambda_1\rangle = \frac{1}{N_1} R_\mu |0\rangle = \frac{1}{N_1} \sum_{\mathrm{ph}} c_{\mathrm{ph}}^{\lambda_1} |(\mathrm{p} \times \mathrm{h}^{-1})^{1^-}\rangle, \tag{16}$$

where R_μ is the c.m. coordinate, $c_{\mathrm{ph}}^{\lambda_1}$ are the unnormalized coefficients

$$c_{\mathrm{ph}}^{\lambda_1} = \sqrt{\frac{4\pi}{9}} \frac{1}{A} \langle \mathrm{p} \| r Y_1 \| \mathrm{h} \rangle, \tag{17}$$

and N_1 is the normalization constant

$$N_1^2 = \sum_{\mathrm{ph}} \left| c_{\mathrm{ph}}^{\lambda_1} \right|^2. \tag{18}$$

The basis states $|\Phi_i\rangle$ obtained by such an orthogonalization procedure are linear combinations of the p-h states $|(\mathrm{p} \times \mathrm{h}^{-1})^{1^-}\rangle$. They must be used to construct and diagonalize the Hamiltonian matrix yielding eigenstates rigorously free of spurious admixtures. These eigenstates recover the standard TDA structure given by Eq. (14) once the states $|\Phi_i\rangle$ are expressed in terms of the original configurations $|(\mathrm{p} \times \mathrm{h}^{-1})^{1^-}\rangle$.

B. Derivation of the *n*-phonon basis

The primary objective of the method is to generate an orthonormal basis of n-phonon states ($n = 1,2,\ldots$) of the form

$$\begin{aligned} |\beta_n\rangle &= \sum_{\lambda\alpha_{n-1}} C_{\lambda\alpha_{n-1}}^{\beta} |(\lambda \times \alpha_{n-1})^{\beta_n}\rangle \\ &= \sum_{\lambda\alpha_{n-1}} C_{\lambda\alpha_{n-1}}^{\beta_n} \{O_\lambda^\dagger \times |\alpha_{n-1}\rangle\}^{\beta_n}, \end{aligned} \tag{19}$$

where the TDA phonon operator $O_\lambda^\dagger$ (14), of energy E_λ, acts on a $(n-1)$-phonon state $|\alpha_{n-1}\rangle$, of energy $E_{\alpha_{n-1}}$, assumed to be known.

The key for generating such a basis is provided by the equations of motion

$$\langle\beta|([H, O_\lambda^\dagger] \times |\alpha\rangle)^\beta = (E_\beta - E_\alpha)\langle\beta|(\lambda \times \alpha)^\beta\rangle, \tag{20}$$

where the subscript n has been omitted for simplicity. Upon applying the Wigner-Eckart theorem, we obtain the equivalent equations

$$\langle\beta\|[H, O_\lambda^\dagger]\|\alpha\rangle = (E_\beta - E_\alpha)\langle\beta\|O_\lambda^\dagger\|\alpha\rangle. \tag{21}$$

We, then, expand the commutator and invert Eq. (14) to express the p-h operators, appearing in the expanded commutator, in terms of the phonon operators $O_\lambda^\dagger$. The outcome of this action is [43]

$$\sum_{\lambda'\alpha'} \mathcal{A}_{\lambda\alpha\lambda'\alpha'}^{\beta} X_{\lambda'\alpha'}^{\beta} = E_\beta X_{\lambda\alpha}^{\beta}, \tag{22}$$

where X defines the amplitude

$$X_{\lambda\alpha}^{\beta} = \langle\beta\|O_\lambda^\dagger\|\alpha\rangle, \tag{23}$$

and $\mathcal{A}$ is a matrix of the simple structure

$$\mathcal{A}_{\lambda\alpha\lambda'\alpha'}^{\beta} = (E_\lambda + E_\alpha)\delta_{\lambda\lambda'}\delta_{\alpha\alpha'} + \sum_\sigma W(\beta\lambda'\alpha\sigma;\alpha'\lambda)\mathcal{V}_{\lambda\alpha\lambda'\alpha'}^{\sigma}. \tag{24}$$

Here, the phonon-phonon potential is given by

$$\mathcal{V}_{\lambda\alpha\lambda'\alpha'}^{\sigma} = \sum_{rs} \mathcal{V}_{\lambda\lambda'}^{\sigma}(rs)\rho_{\alpha\alpha'}^{(n)}([r \times s]^\sigma), \tag{25}$$

where the labels (rs) run over particle ($rs = pp'$) and hole ($rs = hh'$) states. In the above equation, we have introduced the n-phonon density matrix

$$\rho_{\alpha\alpha'}^{(n)}([r \times s]^\sigma) = \langle\alpha_n'\|[a_r^\dagger \times b_s]^\sigma\|\alpha_n\rangle \tag{26}$$

and the potential

$$\mathcal{V}_{\lambda\lambda'}^{\sigma}(rs) = \sum_{tq} \rho_{\lambda\lambda'}([q \times t]^\sigma) F_{qtrs}^{\sigma}, \tag{27}$$

where $\rho_{\lambda\lambda'}$ is the TDA density matrix (15).

The phonon matrix $\mathcal{A}_{\lambda\alpha\lambda'\alpha'}^{\beta}$ is formally equivalent to the TDA matrix $A_{\mathrm{php'h'}}^{\lambda}$ [43]. The first is deduced from the second by replacing the p-h energies with the sum of phonon energies and the p-h interaction with the phonon-phonon potential (25).

Equation (22) is not an eigenvalue equation yet. We have first to expand the amplitudes X (23) in terms of the expansion coefficients $C_{\lambda\alpha}^{\beta}$ of the states $|\beta\rangle$ (19) obtaining

$$X_{\lambda\alpha}^{\beta} = \sum_{\lambda'\alpha'} \mathcal{D}_{\lambda\alpha\lambda'\alpha'}^{\beta} C_{\lambda'\alpha'}^{\beta}, \tag{28}$$

where $\mathcal{D}$ is the metric or overlap matrix given by

$$\begin{aligned} \mathcal{D}_{\lambda\alpha\lambda'\alpha'}^{\beta} &= \langle(\lambda \times \alpha)^\beta|(\lambda' \times \alpha')^\beta\rangle \\ &= \delta_{\lambda\lambda'}\delta_{\alpha\alpha'} + \sum_\gamma W(\alpha'\lambda\lambda'\alpha;\gamma\beta) X_{\lambda'\gamma}^{\alpha} X_{\lambda\gamma}^{\alpha'} - (-)^{\alpha+\beta+\lambda} \\ &\quad \times \sum_{rs\sigma} W(\lambda'\lambda\alpha'\alpha;\sigma\beta)\rho_{\lambda\lambda'}([r \times s]^\sigma)\rho_{\alpha'\alpha}([r \times s]^\sigma), \end{aligned} \tag{29}$$

and $X_{\lambda\gamma}^{\alpha} = \langle\alpha_{n-1}\|O_\lambda^\dagger\|\gamma_{n-2}\rangle$. The overlap matrix $\mathcal{D}$ reestablishes the Pauli principle by reintroducing the exchange terms among different phonons, in addition to the Kronecker product.

By inserting the expansion (28) into Eq. (22), we get

$$\begin{aligned} \sum_{\lambda'\alpha'} \mathcal{H}_{\lambda\alpha\lambda'\alpha'}^{\beta} C_{\lambda'\alpha'}^{\beta} &= \sum_{\lambda'\alpha'} (A\mathcal{D})_{\lambda\alpha\lambda'\alpha'}^{\beta} C_{\lambda'\alpha'}^{\beta} \\ &= E_\beta \sum_{\lambda'\alpha'} \mathcal{D}_{\lambda\alpha\lambda'\alpha'}^{\beta} C_{\lambda'\alpha'}^{\beta}. \end{aligned} \tag{30}$$

These are a set of generalized eigenvalue equations in the overcomplete basis states $|(\lambda \times \alpha)^\beta\rangle$.

Following a procedure [41,42] based on the Cholesky decomposition method, we select a basis of linear independent states $|(\lambda \times \alpha)^\beta\rangle$ spanning the physical subspace of the correct dimensions $N_n < N_r$ and construct a $N_n \times N_n$ nonsingular

matrix $\mathcal{D}_n$. By left multiplication in the N_n-dimensional subspace we get from Eq. (30)

$$\left[\mathcal{D}_n^{-1}\mathcal{H}\right]C = \left[\mathcal{D}_n^{-1}(\mathcal{A}\,\mathcal{D})\right]C = EC. \tag{31}$$

This equation determines only the coefficients $C^{\beta}_{\lambda\alpha}$ of the N_n-dimensional physical subspace. The remaining redundant $N_r - N_n$ coefficients are undetermined and, therefore, can be safely put equal to zero.

The eigenvalue problem within the n-phonon subspace is thereby solved exactly and yields a basis of orthonormal correlated n-phonon states of the form (19).

Because recursive formulas hold for all quantities entering $\mathcal{A}$ and $\mathcal{D}$, it is possible to solve the eigenvalue equations iteratively starting from the TDA phonons $|\alpha_1\rangle = |\lambda\rangle$ and, thereby, generate a set of orthonormal multiphonon states $\{|0\rangle, |\alpha_1\rangle, |\alpha_2\rangle, \ldots, |\alpha_n\rangle, \ldots\}$ of the form (19).

C. Eigenvalue problem in the multiphonon basis

The multiphonon basis $\{|\alpha_n\rangle\}$ is finally used to solve the eigenvalue equations in the multiphonon space

$$\sum_{n'\beta_{n'}}\left[\left(E_{\alpha_n} - \mathcal{E}_\nu\right)\delta_{nn'}\delta_{\alpha_n\beta_{n'}} + \mathcal{V}_{\alpha_n\beta_{n'}}\right]\mathcal{C}^{(\nu)}_{\beta_{n'}} = 0, \tag{32}$$

where the potential has the structure

$$\mathcal{V}_{\alpha_n\beta_{n'}} = \delta_{n'(n+1)}\mathcal{V}_{\alpha_n\beta_{n'}} + \delta_{n'(n+2)}\mathcal{V}_{\alpha_n\beta_{n'}}. \tag{33}$$

For $n' = n+1$, the matrix elements are

$$\mathcal{V}_{\alpha_n\beta_{n+1}} = \langle\beta_{n+1}|V|\alpha_n\rangle = \sum_{\sigma\gamma_n}\mathcal{V}^{\sigma}_{\alpha_n\gamma_n}X^{(\beta_{n+1})}_{\sigma\gamma_n}, \tag{34}$$

where

$$\mathcal{V}^{\sigma}_{\alpha_n\gamma_n} = [\alpha_n]^{-1}(-)^{\alpha_n+\gamma_n+\sigma}\sum_{rs}\mathcal{F}^{\sigma}_{rs}\rho^{(n)}_{\alpha\gamma}([r\times s]_\sigma) \tag{35}$$

and

$$\mathcal{F}^{\sigma}_{rs} = \sum_{\rm ph} c^{\sigma}_{\rm ph}F^{\sigma}_{{\rm ph}rs}. \tag{36}$$

For $n' = n+2$ we have

$$\begin{aligned}\mathcal{V}_{\alpha_n\beta_{n+2}} &= \langle\beta_{n+2}|V|\alpha_n\rangle \\ &= [\alpha_n]^{-1}\sum_{\sigma\sigma'\gamma_{n+1}}(-)^{\alpha_n+\gamma_{n+1}+\sigma}X^{\beta_{n+2}}_{\sigma\gamma_{n+1}}X^{\gamma_{n+1}}_{\sigma'\alpha_n}\mathcal{V}_{\sigma\sigma'},\end{aligned} \tag{37}$$

where

$$\mathcal{V}_{\sigma\sigma'} = \delta_{J_\sigma J_{\sigma'}}\frac{1}{4}\sum_{\rm php'h'}F^{J_\sigma}_{\rm php'h'}c^{\sigma}_{\rm ph}c^{\sigma'}_{\rm p'h'}. \tag{38}$$

The solution of Eqs. (32) yields the final eigenvalues $\mathcal{E}_\nu$ and the corresponding eigenfunctions

$$|\Psi_\nu\rangle = \sum_{n\alpha_n}\mathcal{C}^{(\nu)}_{\alpha_n}|\alpha_n\rangle. \tag{39}$$

The entire procedure leading to these eigenstates does not rely on any approximation. For practical applications, however, it might be necessary to truncate the p-h and/or the phonon spaces. The phonon structure, however, allows us to keep both truncations under control.

$|\Psi_\nu\rangle$ can be written as a linear combination of products of n TDA phonons ($n = 0,1,2,3,\ldots$). If the sum is truncated at $n = 2$, it assumes the form of a SRPA wave function [36–39] in its phonon version [40].

Thus, in a space encompassing up to two phonons, our formalism can be considered as the TDA counterpart of SRPA. With respect to our approach, SRPA incorporates effectively the ground-state correlations. The underlying quasiboson approximation, however, produces uncontrollable uncertainties which induce instabilities [38,39].

A connection with the RPA correlated ground state [32,33] can be also established. To this purpose we observe that, if the almost vanishing one-phonon components are neglected, our state assumes the form

$$\begin{aligned}|\Psi_0\rangle &\simeq \mathcal{C}^{(0)}_0|0\rangle + \sum_{\alpha_2}\mathcal{C}^{(0)}_{\alpha_2}|\alpha_2\rangle, \\ &= \mathcal{C}^{(0)}_0|0\rangle + \sum_{\lambda\lambda'}\mathcal{C}^{(0)}_{\lambda\lambda'}|(\lambda\times\lambda')^0\rangle,\end{aligned} \tag{40}$$

where $\mathcal{C}^{(0)}_{\lambda\lambda'} = \sum_{\alpha 2}\mathcal{C}^{(0)}_{\alpha_2}C^{\alpha_2}_{\lambda\lambda'}$ follows from Eq. (19).

We can now imagine of turning our eigenvalue problem into an equivalent one within the one-dimensional HF space. In such a perturbative context, $|\Psi_0\rangle$ is connected to the HF state by a wave operator of the same exponential form derived for the RPA correlated ground state [32,33] and its energy is given by a series of terms describing the propagation of interacting 2p-2h [43].

This series does not include the RPA ring diagrams describing the propagation of np-nh ($n > 2$), which add more attraction to the ground state. However, it contains infinite sets of diagrams, ignored in RPA, describing the p-p and h-h interactions among the Fermionic constituents of the two phonons and producing an overall repulsive contribution. It might be worth pointing out that the RPA formalism relies on the quasiboson approximation, which tends to overestimate the correlation energy to an extent that cannot be quantified easily.

III. NUMERICAL CALCULATIONS

As anticipated in the Introduction, we make use of the *NN* optimized chiral potential NNLO_{opt} determined by fixing the coupling constants at next-to-next-leading order through a new optimization method in the analysis of the phase shifts, which minimizes the effects of the $3N$ forces [24].

A. Ground-state energy and convergence properties

We generate a HF basis in a HO space which includes a variable number of major shells, up to the principal quantum number $N_{\max} = 14$. This allows us to study the stability of the ground-state energy against the variation of the HO frequencies and space dimensions.

An example is given in Fig. 1. In ^{4}He, for $N_{\max}$ sufficiently large, the HF ground-state energy is almost insensitive to the space dimensions, especially at fairly high frequencies ($\hbar\omega \geqslant 16$ MeV). A completely flat stable minimum is reached for $N_{\max} \geqslant 10$ and $\hbar\omega \geqslant 16$ MeV and over the whole frequency range for $N_{\max} = 14$.

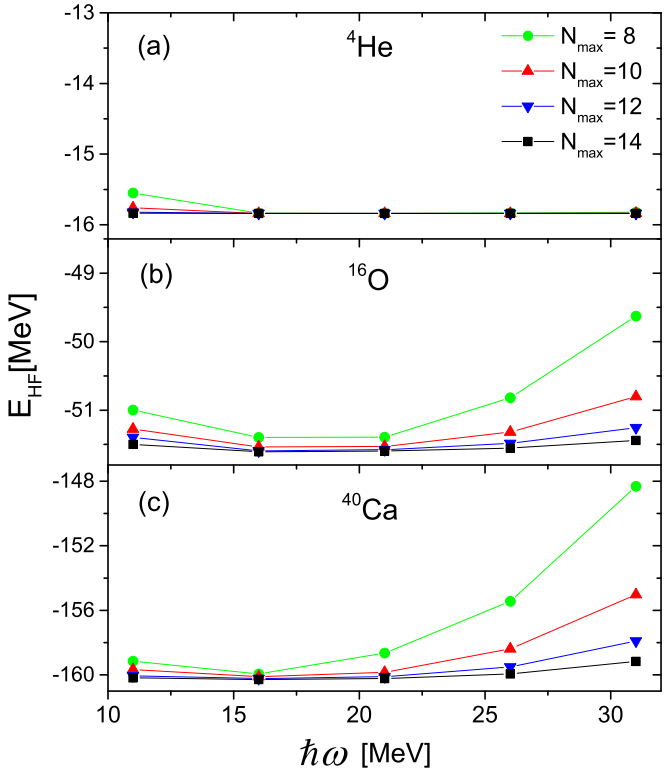

FIG. 1. HF ground-state energy of ^{4}He (a), ^{16}O (b), and ^{40}Ca (c) versus the HO frequencies ω for different HO space dimensions $N_{\max}$.

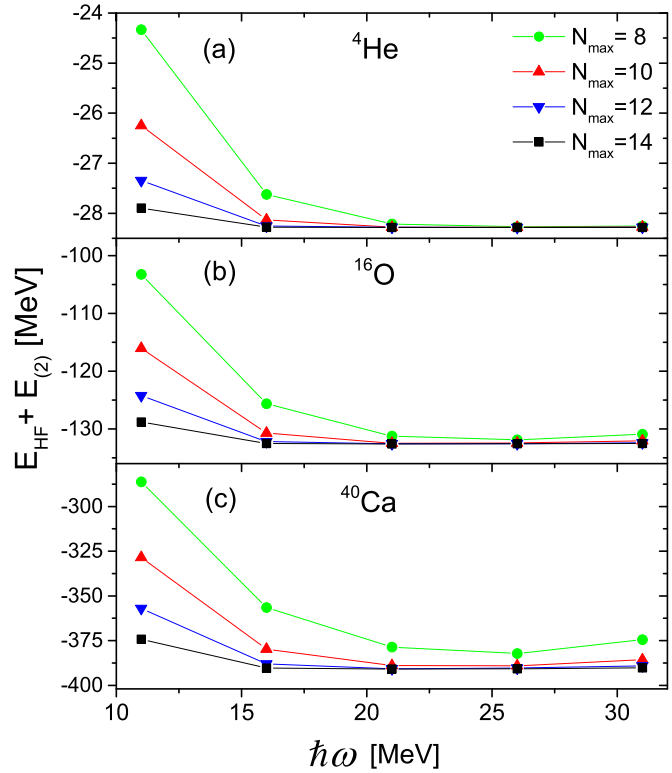

FIG. 2. Ground-state energy of ^{4}He (a), ^{16}O (b), and ^{40}Ca (c) versus the HO frequency ω for different $N_{\max}$ computed in HF plus second-order perturbation theory.

In ^{16}O and ^{40}Ca, the convergence range is rather restricted for $N_{\max} \sim 10$ and is more substantial for $N_{\max} = 14$, $16 \leqslant \hbar\omega \leqslant 25$ MeV, and $10 \leqslant \hbar\omega \leqslant 25$ MeV in ^{16}O and ^{40}Ca, respectively. The HF energy remains close to the minimum with decreasing $N_{\max}$ at low frequencies, just like in ^{4}He, and departs from it more appreciably and faster in the high-frequency sector.

The second-order contribution has a strong impact and spoils the convergence at low frequencies in all three nuclei. In all of them, the total energy converges to the minimum value starting from $\hbar\omega \sim 16$ MeV for $N_{\max} \geqslant 12$ and from $\hbar\omega \sim 21$ MeV for $N_{\max} = 10$ (Fig. 2). The extremal value tends to stabilize in the region of high frequencies independently of the mass number.

The strong influence of the perturbative term on the convergence properties can be understood by observing that (a) the particle states come into play directly into the perturbative term and increase in number enormously with $N_{\max}$, (b) the second-order corrections are, in general, comparable with or larger than the HF energies. They account for ∼44%, ∼61%, and ∼59% of the theoretical binding energy in ^{4}He, ^{16}O, and ^{40}Ca, respectively. These large contributions determine slight overbindings with the exception of ^{4}He (Table I).

Perturbation theory has a (too) strong impact on the energies of all nuclei throughout the periodic table. We have evaluated the binding energies of a selected set of doubly magic and semimagic nuclei for $N_{\max} = 14$ and different frequencies. The systematic presented in Fig. 3 shows that the perturbative corrections are dominant and cause increasing overbinding with increasing mass number. These corrections induce also a dependence on the HO frequency, even for $N_{\max} = 14$, especially in the heavy nuclei.

An analogous trend of the perturbative energy corrections, all along the chain of nuclei investigated, was obtained in Ref. [25], when a $NN + 3N$ full chiral interaction is used.

This analogy confirms that the NNLO$_{\rm opt}$ [24] absorbs effectively a substantial fraction of the contribution of the chiral $3N$ forces [16] to the ground-state energy.

In the non-perturbative treatment, we use all TDA phonons allowed by the dimensions of the p-h space for each $N_{\max}$ to generate the correlated two-phonon basis states $|\alpha_2\rangle$ [Eq. (19)] through Eqs. (31). We then adopt the full basis $\{|0\rangle, |\lambda\rangle, |\alpha_2\rangle\}$ to solve the eigenvalue equations (32) obtaining thereby all eigenstates allowed by the multiphonon space. Only the lowest eigenstate Ψ_0 [Eq. (40)] is the object of our interest here.

A systematic study of the convergence properties of the EMPM ground-state energy would be too time consuming. They are investigated thoroughly only in ^{4}He and ^{16}O.

TABLE I. Binding energies per nucleon. The EMPM value for ^{40}Ca was obtained for $N_{\max} = 8$, which is not an extremal point.

	BE/A (MeV)			
$^A X$	HF	PT	EMPM	Exp.
^{4}He	3.96	7.07	6.67	7.07
^{16}O	3.22	8.29	6.77	7.98
^{40}Ca	4.00	9.77	7.02	8.55

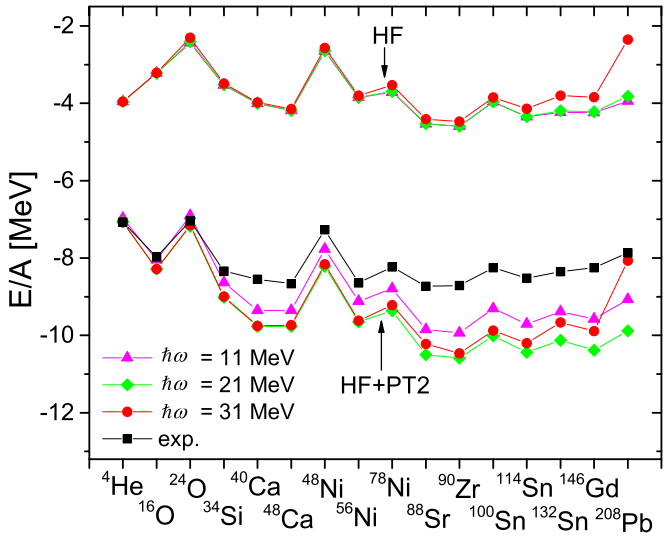

FIG. 3. Systematic of ground-state energy computed in HF and second-order perturbation theory. The calculations are performed for $N_{\max} = 14$ and different HO frequencies ω.

As shown in Figs. 4, the minimum is reached over a wide frequency range for $N_{\max} \geqslant 10$. The most striking differences between second-order perturbation theory and EMPM emerging from Figs. 3 and 4 is that the absolute energies obtained in the EMPM are ∼1.6 and ∼24 MeV smaller in ^{4}He and ^{16}O, respectively, indicating that the higher-order terms have an appreciable repulsive effect. In the nonperturbative approach, the two-phonon contribution represents the ∼40% and ∼53% of the total energy in ^{4}He and ^{16}O, respectively, and induces an underestimation of their binding energy per nucleon (Table I).

According to a calculation based on the RPA correlated ground state, the corrections to the second-order energy coming from the higher-order ring diagrams are attractive [35].

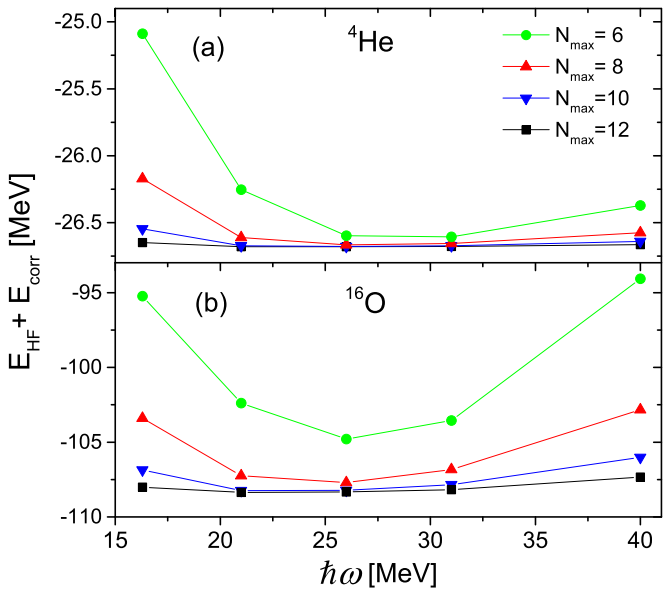

FIG. 4. The EMPM ground-state energy of ^{4}He (a) and ^{16}O (b) versus the HO frequency ω for different $N_{\max}$.

We may therefore infer from this result that the repulsive contribution comes entirely from the p-p and h-h interactions among phonons, which are missing in the RPA calculation.

B. Ground-state radius and convergence properties

To evaluate the point proton root-mean-square (r.m.s.) radius we use the intrinsic operator [50]

$$r_p^2 = \frac{1}{Z}\sum_{i=1,Z}(\mathbf{r}_i - \mathbf{R}_{\text{c.m.}})^2. \tag{41}$$

For $N = Z$, it becomes

$$r_p^2 = \left(1 - \frac{1}{A}\right)\frac{1}{Z}\sum_{i=1,Z}\mathbf{r}_i^2 - \frac{2}{A^2}\sum_{i<j}\mathbf{r}_i \cdot \mathbf{r}_j. \tag{42}$$

Disregarding the terms in $\mathbf{r}_i \cdot \mathbf{r}_j$, in line with Ref. [29], we get

$$r_p^2 = \left(1 - \frac{1}{A}\right)\frac{1}{Z}\sum_{i=1,Z}\mathbf{r}_i^2. \tag{43}$$

The charge radius is deduced from the standard expression [8]

$$\langle r_{ch}^2\rangle = \langle r_p^2\rangle + R_p^2 + \frac{N}{Z}R_n^2 + \frac{3\hbar^2}{4m_p^2c^2}, \tag{44}$$

where $R_p = 0.8775(51)$ fm, $R_n^2 = 0.1149(27)$ fm^2, and $\frac{3\hbar^2}{4m_p^2c^2} \sim 0.033$ fm^2.

In the EMPM, we use the wave function Ψ_0 (40) to obtain

$$\langle r_p^2\rangle = \langle\Psi_0|r_p^2|\Psi_0\rangle = \langle r_p^2\rangle_{\text{HF}} + \langle r_p^2\rangle_{\text{corr}}, \tag{45}$$

where $\langle r_p^2\rangle_{\text{HF}}$ is the HF value and $\langle r_p^2\rangle_{\text{corr}}$ is the contribution coming from the two-phonon correlations. This is given by

$$\langle r_p^2\rangle_{\text{corr}} = \sum_{\alpha\beta}\delta_{J_\alpha J_\beta}\delta_{J_\alpha 0}\mathcal{C}_\alpha^{(0)}\mathcal{C}_\beta^{(0)}\mathcal{M}_{\alpha\beta}^{(0)}, \tag{46}$$

where

$$\mathcal{M}_{\alpha\beta}^{(0)} = \sum_{rs}\langle r\|r_p^2\|s\rangle\langle\beta\|(a_r^\dagger \times b_s)^0\|\alpha\rangle. \tag{47}$$

In analogy with the energy, the HF point proton radius reaches the convergence over a wide frequency interval for $N_{\max} \geqslant 10$ in ^{4}He and ^{16}O (Fig. 5). The HF radii are systematically smaller than the empirical ones throughout the whole periodic table (Fig. 6).

The convergence of the radius computed in the EMPM is as fast as in the HF case (Fig. 7). The contribution of the two-phonon correlations is much more modest than in the case of the energy and is far from filling the gap with the empirical values (Table II).

The underestimation of the binding energies and radii indicates that the two-phonon correlations are not strong enough. They account for ∼22% of the total wave function, which is dominated by the HF component (∼78%).

Apparently, HF and two-phonon states are not admixed sufficiently by the phonon coupling. The weakness of such a coupling may be attributable to the HF spectrum. The levels above the Fermi surface generated by NNLO$_{\text{opt}}$, or other potentials as well [28,48,51], are too far apart, especially at high energies. A smoother HF level scheme would yield a more

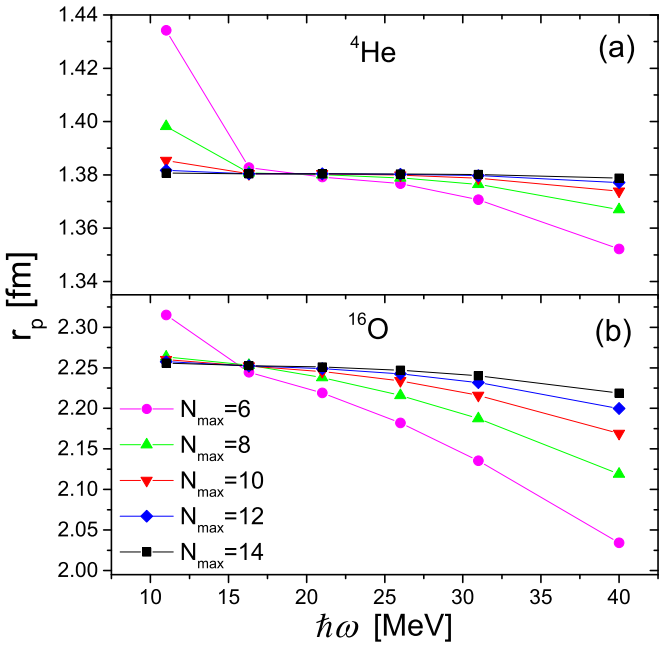

FIG. 5. HF point proton radius versus the HO frequency ω for different N_{max} in ^{4}He (a) and ^{16}O (b).

compact TDA spectrum and, therefore, should strengthen the phonon coupling.

Acting at the HF level only is not sufficient. More complex multiphonon configurations, capable of shifting down the two-phonon levels and rendering more effective their coupling to the HF state, are to be considered. The positive-parity three-phonon states are expected to produce, through their coupling, a fragmentation of the two-phonon spectrum. It is necessary to check if it produces a downward shift of its levels.

We expect a strong effect from the four-phonon states. An indirect confirm of their importance comes from the CC [1,5]

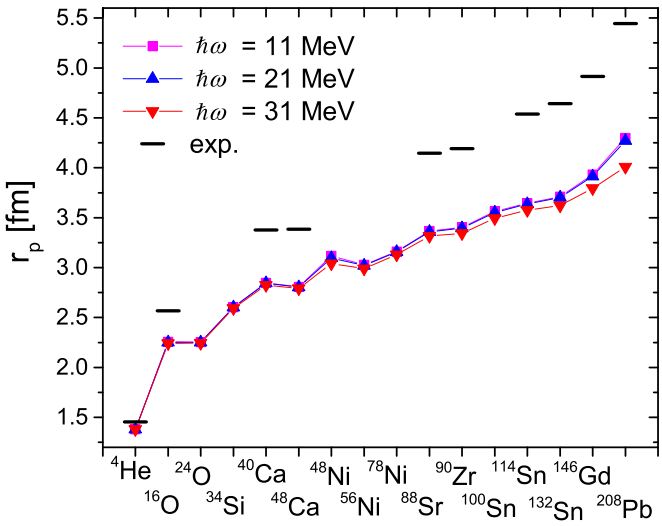

FIG. 6. Systematic of root-mean-square point proton radii computed in HF. The calculations are performed for $N_{max} = 14$ and different HO frequencies ω. The experimental data are from Ref. [49].

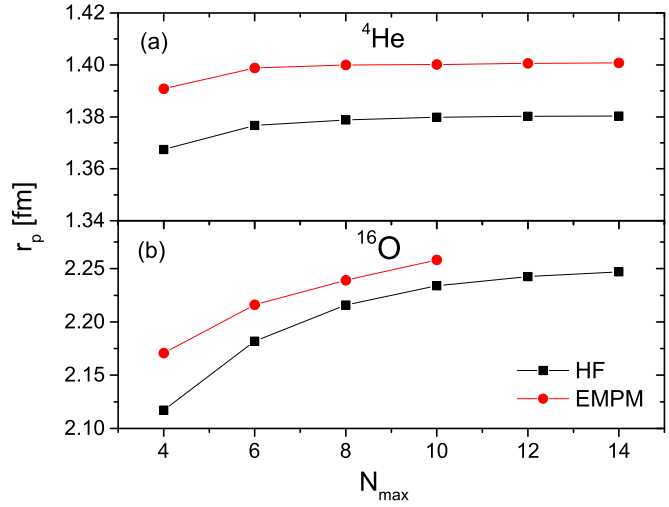

FIG. 7. HF and EMPM point proton radii of ^{4}He (a) and ^{16}O (b) versus N_{max} for fixed frequency ($\hbar\omega = 26$ MeV).

and IM-SRG [14,15] theories, where (4p-4h) contributions are effectively accounted for to some extent.

That the coupling to four-phonon states is expected to be strong can be inferred from the formula

$$\langle\alpha_4|V|\alpha_2\rangle = \sum_{\gamma_2}\langle\alpha_4|(\alpha_2 \times \gamma_2)^0\rangle\langle\gamma_2|V|0\rangle, \qquad (48)$$

which correlates closely the four-phonon to two-phonon coupling with the strong coupling between two phonons and the HF vacuum.

Generating a basis of correlated four-phonon states in a large space is prohibitive. It would require the calculation of a huge number of density matrices (26). Thus, a preliminary condition for achieving our task consists in the possibility of truncating the multiphonon space at a negligible detriment of the accuracy of the calculation.

As shown in Fig. 8, the convergence with the number of two-phonon states is slow. Although the components with the largest amplitudes are below ∼100 MeV, the tiny components are in a huge number and give a large contribution to the wave function. Thus, a mere truncation of the basis according to the energy is not efficient.

We need to resort to a more sophisticated importance sampling [52], shown to be effective in large-scale shell-model calculations [53,54], and check if the sampled basis is sufficiently restricted to allow the access to subspaces with a larger number of phonons. Preliminary calculations

TABLE II. Point proton radii. The experimental data are from Ref. [49]. The EMPM value in ^{16}O was obtained for the nonextremal point $N_{max} = 10$.

	r_p (fm)		
$^A X$	HF	EMPM	Exp.
^{4}He	1.38	1.40	1.46
^{16}O	2.25	2.26	2.57

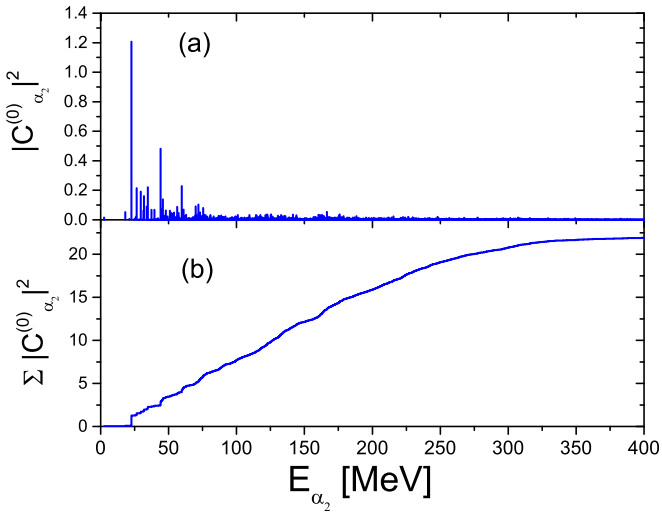

FIG. 8. Squared amplitudes (multiplied by 100) of the two-phonon components (a) of the ground state in ^{16}O and their running sum (b).

are encouraging. They indicate that the ground-state energy can be well approximated by using ∼30% of the basis states.

A further simplification may consist in neglecting the interaction among phonons [Eq. (25)] when we solve Eq. (30) to generate the four-phonon states $|\alpha_4\rangle$. This interaction induces only a reshuffling of levels falling at energy too high to have appreciable consequences on the coupling. A quantitative test of this approximation, however, requires rather elaborate calculations.

IV. CONCLUSIONS

The main conclusion to be drawn from our calculation is that (a) a stable HF and, especially, EMPM energy minimum is obtained only if the HF basis is determined using a large number of HO major shells at specific frequencies, (b) a large fraction of the ground-state correlation energy comes from the two-phonon (2p-2h) configurations, (c) the terms beyond second order are appreciable and have a repulsive effect, (d) the attractive two-phonon contribution is not sufficient to reproduce the experimental binding energies and radii, and (e) at least four-phonon (4p-4h) configurations are needed to produce the missing attractive contribution.

Though the formalism is valid for any number of phonons, its numerical implementation in a multiphonon space encompassing also the four-phonon basis is unfeasible if we pretend to use all phonons generated by the full p-h basis. We have to rely on their correlated nature and investigate if, though starting from a p-h space of large dimensions, the set of *relevant* phonons is sufficiently restricted to allow us to generate the four-phonon states in a drastically truncated space.

ACKNOWLEDGMENTS

This work was partly supported by the Czech Science Foundation (Czech Republic), Grant No. P203-13-07117S. Two of the authors (F. Knapp and P. Veselý) thank the INFN (Italy) for financial support. Highly appreciated was the access to computing and storage facilities provided by the Meta Centrum under Program No. LM2010005 and the CERIT-SC under the program Centre CERIT Scientific Cloud, part of the Operational Program Research and Development for Innovations, Registration No. CZ.1.05/3.2.00/08.0144.

[1] G. Hagen, T. Papenbrock, M. Hjorth-Jensen, and D. J. Dean, Rep. Prog. Phys. **77**, 096302 (2014).
[2] P. Navrátil, S. Quaglioni, I. Stetcu, and B. R. Barrett, J. Phys. G: Nucl. Part. Phys. **36**, 083101 (2009).
[3] P. Maris, J. P. Vary, and A. M. Shirokov, Phys. Rev. C **79**, 014308 (2009).
[4] B. R. Barrett, P. Navrátil, and J. P. Vary, Prog. Part. Nucl. Phys. **69**, 131 (2013).
[5] D. J. Dean and M. Hjorth-Jensen, Phys. Rev. C **69**, 054320 (2004).
[6] G. Hagen, T. Papenbrock, D. J. Dean, and M. Hjorth-Jensen, Phys. Rev. C **82**, 034330 (2010).
[7] G. Hagen, M. Hjorth-Jensen, G. R. Jansen, R. Machleidt, and T. Papenbrock, Phys. Rev. Lett. **108**, 242501 (2012).
[8] A. Ekström, G. R. Jansen, K. A. Wendt, G. Hagen, T. Papenbrock, B. D. Carlsson, C. Forssén, M. Hjorth-Jensen, P. Navrátil, and W. Nazarewicz, Phys. Rev. C **91**, 051301 (2015).
[9] S. Binder, J. Langhammer, A. Calci, and R. Roth, Phys. Lett. B **736**, 119 (2014).
[10] A. Signoracci, T. Duguet, G. Hagen, and G. R. Jansen, Phys. Rev. C **91**, 064320 (2015).
[11] K. Tsukiyama, S. K. Bogner, and A. Schwenk, Phys. Rev. Lett. **106**, 222502 (2011).
[12] H. Hergert, S. K. Bogner, S. Binder, A. Calci, J. Langhammer, R. Roth, and A. Schwenk, Phys. Rev. C **87**, 034307 (2013).
[13] H. Hergert, S. K. Bogner, T. D. Morris, S. Binder, A. Calci, J. Langhammer, and R. Roth, Phys. Rev. C **90**, 041302(R) (2014).
[14] T. D. Morris, N. M. Parzuchowski, and S. K. Bogner, Phys. Rev. C **92**, 034331 (2015).
[15] H. H. Hergert, S. K. Bogner, T. D. Morris, A. Schwenk, and K. Tsukiyama, Phys. Rep. **621**, 165 (2016).
[16] R. Machleidt and D. R. Entem, Phys. Rep. **503**, 1 (2011).
[17] J. W. Holt, N. Kaiser, and W. Weise, Phys. Rev. C **81**, 024002 (2010).
[18] K. Hebeler, S. K. Bogner, R. J. Furnstahl, A. Nogga, and A. Schwenk, Phys. Rev. C **83**, 031301(R) (2011).
[19] P. Maris, J. P. Vary, and P. Navrátil, Phys. Rev. C **87**, 014327 (2013).
[20] T. Otsuka, T. Suzuki, J. D. Holt, A. Schwenk, and Y. Akaishi, Phys. Rev. Lett. **105**, 032501 (2010).
[21] A. Cipollone, C. Barbieri, and P. Navrátil, Phys. Rev. Lett. **111**, 062501 (2013).
[22] H. Hergert, S. Binder, A. Calci, J. Langhammer, and R. Roth, Phys. Rev. Lett. **110**, 242501 (2013).
[23] V. Lapoux, V. Somá, C. Barbieri, H. Hergert, J. D. Holt, and S. R. Stroberg, Phys. Rev. Lett. **117**, 052501 (2016).

[24] A. Ekström, G. Baardsen, C. Forssén, G. Hagen, M. Hjorth-Jensen, G. R. Jansen, R. Machleidt, W. Nazarewicz, T. Papenbrock, J. Sarich *et al.*, Phys. Rev. Lett. **110**, 192502 (2013).
[25] A. Tichai, J. Langhammer, S. Binder, and R. Roth, Phys. Lett. B **756**, 283 (2016).
[26] R. Roth and J. Langhammer, Phys. Lett. B **683**, 272 (2010).
[27] L. Coraggio, N. Itaco, A. Covello, A. Gargano, and T. T. S. Kuo, Phys. Rev. C **68**, 034320 (2003).
[28] R. Roth, P. Papakonstantinou, N. Paar, H. Hergert, T. Neff, and H. Feldmeier, Phys. Rev. C **73**, 044312 (2006).
[29] B. S. Hu, F. R. Xu, Z. H. Sun, J. P. Vary, and T. Li, Phys. Rev. C **94**, 014303 (2016).
[30] G. E. Brown and G. Jacob, Nucl. Phys. **42**, 177 (1963).
[31] E. A. Sanderson, Phys. Lett. **19**, 141 (1965).
[32] D. J. Rowe, Phys. Rev. **175**, 1283 (1968).
[33] P. J. Ellis, Nucl. Phys. A **155**, 625 (1970).
[34] E. Heinz, H. Müther, and H. A. Mavromatis, Nucl. Phys. A **587**, 77 (1995).
[35] C. Barbieri, N. Paar, R. Roth, and P. Papakonstantinou, arXiv:nucl-th/0608011v1.
[36] C. Yannouleas, Phys. Rev. C **35**, 1159 (1987).
[37] S. Drożdż, S. Nishizaki, J. Speth, and J. Wambach, Phys. Rep. **197**, 1 (1990).
[38] P. Papakonstantinou and R. Roth, Phys. Rev. C **81**, 024317 (2010).
[39] P. Papakonstantinou, Phys. Rev. C **90**, 024305 (2014).
[40] D. Gambacurta, F. Catara, M. Grasso, M. Sambataro, M. V. Andrés, and E. G. Lanza, Phys. Rev. C **93**, 024309 (2016).
[41] F. Andreozzi, F. Knapp, N. Lo Iudice, A. Porrino, and J. Kvasil, Phys. Rev. C **75**, 044312 (2007).
[42] F. Andreozzi, F. Knapp, N. Lo Iudice, A. Porrino, and J. Kvasil, Phys. Rev. C **78**, 054308 (2008).
[43] D. Bianco, F. Knapp, N. Lo Iudice, F. Andreozzi, and A. Porrino, Phys. Rev. C **85**, 014313 (2012).
[44] D. Bianco, F. Knapp, N. Lo Iudice, F. Andreozzi, A. Porrino, and P. Veselý, Phys. Rev. C **86**, 044327 (2012).
[45] F. Knapp, N. Lo Iudice, P. Veselý, F. Andreozzi, G. De Gregorio, and A. Porrino, Phys. Rev. C **92**, 054315 (2015).
[46] F. Knapp, N. Lo Iudice, P. Veselý, F. Andreozzi, G. De Gregorio, and A. Porrino, Phys. Rev. C **90**, 014310 (2014).
[47] G. De Gregorio, F. Knapp, N. Lo Iudice, and P. Vesely, Phys. Rev. C **93**, 044314 (2016).
[48] D. Bianco, F. Knapp, N. Lo Iudice, P. Veselý, F. Andreozzi, G. De Gregorio, and A. Porrino, J. Phys. G: Nucl. Part. Phys. **41**, 025109 (2014).
[49] I. Angeli and K. P. Marinova, At. Data Nucl. Data Tables **99**, 69 (2013).
[50] G. P. Kamuntavičius, Phys. Rev. C **56**, 191 (1997).
[51] H. Hergert, P. Papakonstantinou, and R. Roth, Phys. Rev. C **83**, 064317 (2011).
[52] F. Andreozzi, N. Lo Iudice, and A. Porrino, J. Phys. G: Nucl. Part. Phys. **29**, 2319 (2003).
[53] D. Bianco, F. Andreozzi, N. Lo Iudice, A. Porrino, and F. Knapp, Phys. Rev. C **85**, 034332 (2012).
[54] D. Bianco, N. Lo Iudice, F. Andreozzi, A. Porrino, and F. Knapp, Phys. Rev. C **86**, 044325 (2012).